PBEE assessment of RC frames with traditional and sliding-joint infills

COMPDYN 2019
7th ECCOMAS Thematic Conference on
Computational Methods in Structural Dynamics and Earthquake Engineering
M. Papadrakakis, M. Fragiadakis (eds.)
Crete, Greece, 24–26 June 2019

PBEE ASSESSMENT OF RC FRAMES WITH TRADITIONAL AND SLIDING-JOINT INFILLS

V. Bolis[1], F. Basone[2], F. Di Trapani[3], M. Preti[1]

[1]Università degli Studi di Brescia. Department of Civil, Environmental, Architectural Engineering and Mathematics. Via Branze 43, 25123 Brescia, Italy.
e-mail: {valentino.bolis, marco.preti}@unibs.it

[2]Università degli Studi di Enna "Kore". Facoltà di Ingegneria e Architettura.
Cittadella Universitaria, 94100 Enna, Italy.
e-mail: francesco.basone@unikore.it

[3]Politecnico di Torino. Dipartimento di Ingegneria Strutturale, Edile e Geotecnica.
Corso Duca degli Abruzzi, 24, 10128 Turin, Italy.
e-mail: fabio.ditrapani@polito.it

Abstract

In reinforced concrete (RC) multi-storey buildings, the important role of the seismic interaction of structural frames with masonry infills has been revealed by several earthquakes and investigated by many authors. Recently, several innovative infill solutions have been proposed to mitigate such interaction, which could result in widespread damage in both the masonry and the RC structure and sometimes jeopardize the building stability and the occupants' safety. One solution consists in the partitioning of the masonry infill into several sub-panels, relatively sliding along specific joints. This paper investigates the seismic performance assessment of this technological solution in the framework of performance base earthquake engineering. A two-dimensional five-storey RC seismic-resistant frame is selected as case study and the performance is assessed by comparing the responses of the same structure infilled with different solutions, made of sliding joints or traditional masonry, or in the bare configuration. Incremental Dynamic Analyses (IDA) is used for the probabilistic determination of fragility curves of the structures. Results show the seismic fragility and reliability of the different investigated structures, especially addressing the probabilities of occurrence of damage at different limit states and quantifying the associated expected annual loss.

Keywords: seismic reliability, sliding-joints infills, expected annual loss, infilled frames, performance based earthquake engineering.

1 INTRODUCTION

Post-earthquake damage analyses have shown that a consistent part of the reparation costs of reinforced concrete (RC) buildings is related to reparation and/or strengthening of masonry infills and partition walls [1-3], which generally suffer significant damage even in the case of moderate earthquakes. In fact, despite their effectiveness in terms of thermal, acoustic, fire and durability performance, traditional masonry infills are characterized by a large in-plane strength and stiffness, combined with a marked brittleness. As a consequence, they could reach their peak strength for low deformation levels, typically induced by moderate intensity earthquakes, thereafter, as the imposed drift increases, infills show in-plane and out-of-plane response degradation, with diffuse cracking and local crushing. In several cases this may evolve into infills out-of-plane collapse, which significantly increases risk for human life [4,5]. Moreover, as shown in many studies [6, 9 among others], traditional infills entail large interaction with the surrounding frame, inducing localized trusts on the frame columns, which could jeopardize their local performance. Based on these observations, it is clear that the presence of traditional infills in the buildings seismic response could result in relevant reparation and downtime costs.

Several studies have been carried out in the last decade in order to develop innovative infill solutions capable of undergoing limited damage when subjected to different levels of interstorey drifts demanded by earthquakes. They can be summarized into two main categories, one providing infill-frame system strengthening (e.g. [10,11]), the other providing the reduction of infill-frame interaction [12-15]. Among the latter, the partitioning of masonry infills with horizontal sliding joints has shown to be an effective solution for reducing infill-frame interaction and limiting the damage to infills even in the case of severe earthquakes. Such technique has been experimentally confirmed [14, 16-18] and investigated in depth by parametric analyses [19] that allowed providing a simplified equivalent strut modelling approach effectively describing the in-plane sliding-joints infilled frame response [20].

In order to assess the potential of the proposed innovative construction technique for the infills in RC framed structures, in the present paper, its seismic performance is compared with that of a traditional masonry infill, within a probabilistic assessment framework merging seismic fragility, reliability and loss assessment during the service life. The study adopts a performance based earthquake engineering (PBEE) approach, which can provide a quantification of the actual gain obtainable by adopting such kind of technological solution. The structural assessment is based on incremental dynamic analysis (IDA) [21] for the determination of fragility curves, specifically defined in order to include limit states at structural and non-structural level. IDA are performed considering a selection of 30 ground motion records scaled, for the different systems, by assuming spectral acceleration at each specified vibration period, $S_a(T_1)$, as intensity measure (IM). The adopted procedure allows comparing fragilities of structural systems having substantially different fundamental vibration periods (e.g. traditionally infilled frames and sliding-joint infilled frames) by integrating the convolution between fragility and hazard functions. Once obtained the fragility curves for the different structural systems, the assessment is moved to reliability by evaluating probabilities of exceeding each limit state. The analysis results are finally used to extend the investigation in terms of expected annual loss associated to each specified limit state, thus allowing the estimation of post-earthquake restoration costs within the service life.

2 PERFORMANCE BASED EARTHQUAKE ENGINEERING ASSESSMENT FRAMEWORK

In the present paper, the PBEE framework is specifically designed to assess seismic performance of infilled frame systems, characterized by different infill configurations. As described by different authors [22-29], performance based earthquake engineering framework is generally made of four main steps: structural analysis, hazard analysis, damage analysis, and loss analysis.

The structural response is obtained by means of the IDA method, which has been recently widely employed by different authors (e.g. [30,31] among others) to obtain a statistical distribution of the intensity measures inducing a limit state, taking into account the ground motions variability. For the IDAs, a set of 30 spectrum-compatible ground motions is selected and scaled in amplitude up to the achievement of the specified limit states defined as: (i) achievement of structural collapses during the analyses or (ii) limit values of engineering demand parameters (EDPs) (e.g. maximum interstorey drifts). In the adopted framework, for each analyzed structure characterized by its own fundamental vibration period (T_1), the selected ground motions are scaled with respect to the spectral acceleration attained in correspondence of T_1, to obtain $S_a(T_1)$ as a common value for each spectrum. The obtained spectra, and the associated records, are then scaled to be adopted as input ground motion in time history analyses.

From IDA results fragility curves for each limit state (defined in the following) can be derived, which express the probability of exceeding a specified limit state as a function of a specified *IM,* quantified by the following expression:

$$P\left[C \le D \mid IM = x\right] = \Phi\left(\frac{ln(x) - \mu_{ln\,x}}{\sigma_{ln\,x}}\right) \tag{1}$$

where $P\left[C \le D \mid IM = x\right]$ is the probability that a ground motion with $IM=x$ will cause the achievement of a limit state, Φ is the standard cumulative distribution function, $ln(x)$ is the natural logarithm of the variable x representing the intensity measure ($S_a(T_1)$) and μ_{lnX} and σ_{lnX} are the mean and the standard deviation of the natural logarithms of the distribution of x, respectively.

Based on fragility curves, reliability analysis can be performed to evaluate the probability (P_f) of exceeding a given limit state in a reference time period (in years), as expressed in Eq. (2).

$$P_f = \int_0^{+\infty} P\left[C \le D \mid IM = x\right] \cdot P\left[x\right] dx \tag{2}$$

where $P[x]$ is the probability of exceeding an $IM=x=S_a(T_1)$ in a specific site in the reference period (50 years) described by a Poisson model as:

$$P\left[x\right] = 1 - e^{\lambda[x]\Delta t} \tag{3}$$

in which $\lambda[x]$ is a function describing the annual rate of exceeding the $IM=x=S_a(T_1)$.

According to Eq. (2), the probability P_f is obtained by integrating the convolution of hazard curves and fragility curves. While the latter represent the probability of a specific structure of period T_1 to exceed a specified limit state, the former are the probability of exceeding the intensity $S_a(T_1)$ in a specific site in the reference service time period (Δt).

Hazard curves are obtained from the hazard analysis of the site, in which spectral ordinates at different vibration periods ($S_a(T_{1,i})$) are calculated for different annual rates of exceedance

(λ), defined as the inverse of the return periods ($\lambda = 1/T_R$). The interpolation of results allows determining the hazard curves, which are site and period dependent. As shown in Fig.1a, since fragility curves are referred to structures with different fundamental periods, a higher fragility not necessarily means higher probability of failure. Under this observation, the evaluation of P_f allows making consistent comparison between structural systems characterized by different vibration periods.

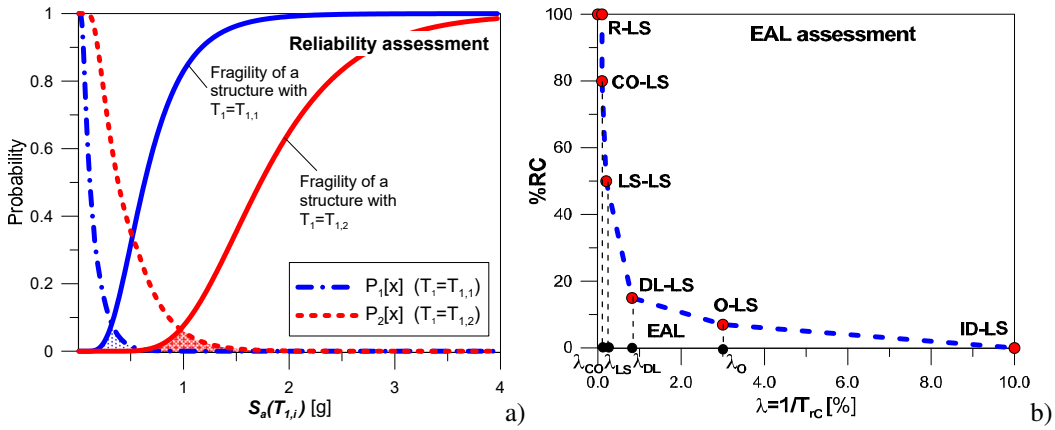

Figure 1: Samples of reliability assessment of two structures having periods T_1 and T_2 (a) and typical EAL curve achievable from the reliabiity assessement (b).

The last stage of the PBEE framework consists in the evaluation of the expected annual loss (EAL) [32, 33]. EAL is determined starting from the performance of the structure for each limit state in terms of annual frequency of exceedance ($\lambda_{LS}=1/T_{rC\text{-}LS}$), being $T_{rC\text{-}LS}$ the capacity return period) and the associated repair costs, expressed as a fraction of reconstruction costs (*%RC*). In the proposed framework, the repair costs associated with each limit states have been assumed as those calibrated in [33]: the total loss or reconstruction limit state (*R-LS*) is assumed equal to 100%, while the *%RC* associated with operational limit state (*O-LS*), damage limit state (*DL-LS*), life safety limit state (*LS-LS*) and collapse limit state (*CO-LS*) are 7%, 15%, 50% and 80%, respectively. The initial damage limit state (*ID-LS*) is conventionally assumed having λ_{ID}=10% and *%RC*=0%. The EAL curve (Fig. 1b) can be obtained by connecting the points (λ_{LS}, *%RC*) representative of each limit state, and the area above the curve represents the EAL. The latter can be simply evaluated as:

$$EAL = \sum_{i=2}^{5} [\,\lambda_{LS(i-1)} - \lambda_{LS(i)}\,] \cdot [\,\%RC_{LS(i)} + \%RC_{LS(i-1)}\,] / 2 + \lambda_{CO} \cdot \%RC_R \qquad (4)$$

As a summary, in the current assessment framework, the following steps are provided:

a. determine the distributions of *IM* at each limit states on IDA curves;
b. determine fragilities for each limit state and the values of the intensity measures having 50% probability of occurrence $\overline{S}_a(T_1)_{LS}$ (mean values);
c. determine the corresponding annual rates of failure (λ_{LS}) through the hazard curves;
d. build EAL curve and evaluate the EAL.

3 THE REFERENCE CASE STUDY STRUCTURE

A 3-bays 5-stories RC frame, extracted from a typical Italian residential building (plan view in Fig. 2a) is selected as reference structure for the present study. The frame (Fig. 2b) is designed according to the Italian building code [34] meeting the design requirements for high

ductility class. Concrete is supposed having nominal strength f_c=25 MPa, steel rebars have nominal yielding strength f_y=560 MPa, while in Table 1 are reported the details of the structural frame elements. The design of horizontal seismic forces is carried out using the design response spectrum obtained for the city of Cosenza (Italy) (soil type C) scaled by a 5.85 behavior factor.

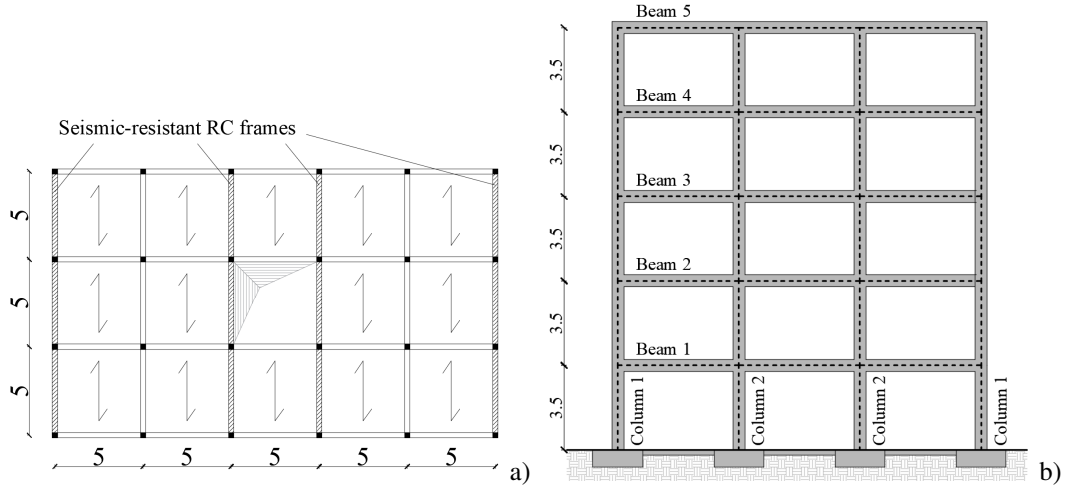

Figure 2: Reference case study building: a) Plan view; b) Selected frame.

BEAMS						
	Geometry		Longitudinal reinforcement		Stirrups	
	b (mm)	*h* (mm)	Bottom	Top	End-zones	Mid-zones
Beam 1	300	450	4ϕ20	2ϕ16+5ϕ20	2ϕ8/100	2ϕ8/150
Beam 2	300	450	4ϕ20	2ϕ16+5ϕ20	2ϕ8/100	2ϕ 8/150
Beam 3	300	450	3ϕ20	3ϕ16+3ϕ20	2ϕ8/100	2ϕ 8/150
Beam 4	300	450	2ϕ20	2ϕ16+2ϕ20	2ϕ8/100	2ϕ 8/150
Beam 5	300	350	2ϕ20	2ϕ16+2ϕ20	2ϕ8/100	2ϕ 8/150
COLUMNS						
	Geometry		Longitudinal reinforcement		Stirrups	
	b (mm)	*h* (mm)			End-zones	Mid-zones
Column 1	450	450	8ϕ20		3ϕ8/100	2ϕ8/150
Column 2	450	450	8ϕ22		3ϕ8/100	2ϕ8/150

Table 1: Geometry and reinforcement details of beams and columns of the selected frame.

Three different configurations for the frame are considered in the following analyses: bare frame (BF), fully infilled frame with traditional masonry infills (TI) and fully infilled frame with infills partitioned by horizontal sliding joints (SJ). For the sake of simplicity no openings are assumed in the infills, whose effect would modify the response of both traditional [35] and sliding joints [36] solid infills. Details of the arrangement of traditional and sliding joint infills are illustrated in Fig. 3. Both the typologies of masonry infills are made of clay hollow blocks with a thickness (t) of 200 mm and 15 mm. Mechanical test results on materials are reported in Table 2. Sliding infills have horizontal sliding joints arranged as proposed by [14] with the introduction of wooden boards able to activate the sliding between two adjacent masonry sub-portions. Wooden boards are supposed to be inserted also at the column-to-infill interface, in order to provide a deformable contact joint preventing masonry from crushing at the sub-panel corners. In particular, in the reference structure the infill with horizontal sliding

joints is considered having lateral wooden boards with halved depth with respect to masonry thickness in order to reduce the contact forces exchanged between the infill and the frame [20].

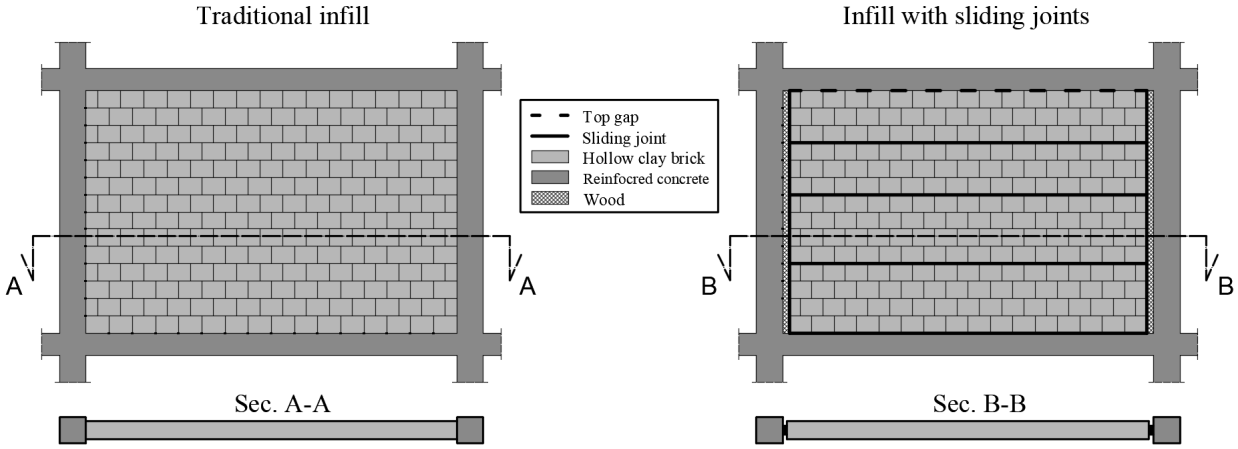

Figure 3: Layout of traditional infills and sliding joint infills.

Material	Compressive Strength (MPa)	Elastic Modulus (MPa)
Masonry prisms: Holes parallel to the load (f_{m2} - E_{m2})	7.28	16148
Masonry prisms: Holes perpend. to the load (f_{m1} - E_{m1})	2.4	4408
Mortar	12.24	18619
Wood perpend. to the grain	2.56	255

Table 2: Material properties from experimental tests [14].

4 MODELING OF THE STRUCTURE AND LIMIT STATES DEFINITION

4.1. Modeling of the infilled RC frame

IDAs on the reference structure have been performed with the Opensees software platform [37]. A distributed plasticity approach is adopted to model the RC frame, using fiber-section beam-column elements characterized by the *Concrete04* material stress-strain model for the cross section fibers. Confinement of concrete is accounted for by dividing cross-sections into effectively confined core fiber and unconfined cover fibers and elements into constant-confinement segments [38-40] in such a way to account for the different transversal reinforcement, while steel rebars are included by means of the *Steel02* material model. The triggering of shear non-linear mechanism is not directly modeled, but possible shear damage or collapses in the frame elements are evaluated a-posteriori.

The in-plane interaction of masonry infills with the RC frame is modeled by adopting a simplified macro-element approach for both TI and SJ infills: equivalent diagonal struts are introduced within the frame bays and calibrated to simulate the infill contribution to the frame lateral strength and stiffness. The struts are compression only truss elements accounting for the degradation during the cyclic in-plane response and connected eccentric with respect to the frame joints in order to model the additional shear demand on the frame elements, induced by the infill-frame interaction. The calibration of the equivalent struts of TI and SJ infills is described in detail in the following sections.

For the traditional infill, a double strut configuration (Fig. 4) is adopted. It provides two parallel struts per each infill diagonal, which are eccentric with respect to the beam-columns joints. Such struts are connected to the frame columns and beams at specified distances from the joint nodes (z_c and z_b, respectively), which are quantified to reproduce both the infill lat-

eral response in terms of strength, stiffness and additional shear action induced in the frame elements. From the results of previous numerical studies [19, 20] such a distance can be set as 1/10 of the frame member length. The response in compression of the struts is defined by *Concrete02* material stress-strain model (parabolic with linear compression softening). The calibration of the struts inelastic response is based on the procedure proposed by [41] for single equivalents strut modelling, which defines the stress–strain curve of the strut through four parameters, namely peak stress (f_{md0}), peak strain (ε_{md0}), ultimate stress (f_{mdu}), and ultimate strain (ε_{mdu}), which are directly linked to geometrical and mechanical properties of the infilled frame. The adopted correlation laws are presented in detail in [41]. A fundamental role in defining the infill in-plane response is acted by the width (w) of the compressed strut activating within the infill in the frame sway mechanism. In the proposed calibration of the single equivalent strut, the width of the strut is determined as proposed in [35].

Based on the stress-strain relationship obtained for the single equivalent the strut, the two eccentric struts in Fig. 4 are calibrated by imposing the equilibrium on the frame according to the following hypotheses:

- the frame is considered hinged in the joints;
- the overall horizontal force at the upper frame beam has to be equivalent to that provided by the single strut;
- the associated resisting forces (F_{md0}, F_{mdu}) in strut B is 80% of that in strut A. This hypothesis is based on the results of several numerical studies (e.g. [19]) demonstrating that shear action generated on the windward column is about the 80% of that on the leeward one.

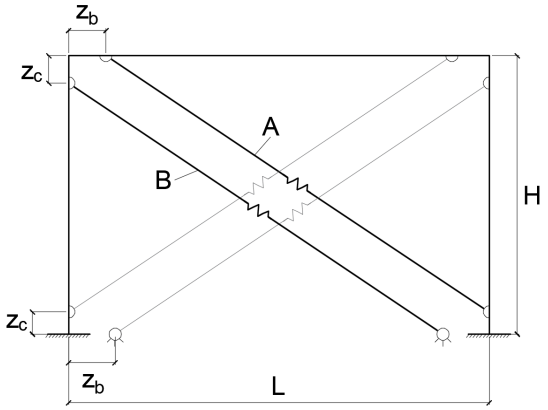

Fig. 4: Simplified equivalent strut model for the traditional infill.

	f_{md0} (MPa)	f_{mdu} (MPa)	ε_{md0} (-)	ε_{md0} (-)	w (mm)	F_{md0} (kN)	F_{mdu} (kN)
Single strut					1170.54	362.40	111.43
Strut A	1.548	0.476	0.00078	0.00733	722.55	223.70	68.78
Strut B					578.04	178.96	55.02

Table 3: Calibration parameters for single and double equivalent strut model for the traditional infill.

As shown in Fig.5a, infill with sliding joints are modeled with two alternative compression-only struts hinged on the columns at a specified distance (z) from the frame joint, as proposed in [20]. The calibration of the strut is based on expressions, allowing, at each deformation level, the simultaneous prediction of the infill lateral strength (ΔF_s) and maximum shear in the columns (V_{max}^{col}), which can be estimated by means of simple equilibrium considerations based only on the geometric and material parameters of the infill. In detail, the

axial stress-strain law of each strut is obtained by means of three axial springs in parallel, calibrated in order to reproduce the analytically obtained force-displacement response (Fig. 5b) and the typical cyclic response of the considered infill typology. The the distance z is calculated as defined in Eq. (15), based on the analytical values of the maximum infill lateral strength and the maximum shear on the columns, at a selected drift level (in this case 2%).

$$z = h\frac{V_{max}^{col} - \Delta F_s}{2V_{max}^{col} - \Delta F_s} \tag{15}$$

The axial constitutive law of the springs is reproduced in the model by using an *Elasto-Plastic Gap* material, which also allows reproducing the cyclic degradation of the infill due to the plastic deformation of the lateral contact joint when increasing the drift level [20]. Table 4 summarizes the calibration parameters of the three springs composing the strut.

Fig. 6 reports the layout of the models of the reference structure adopted in the present study, characterized by different infill configurations.

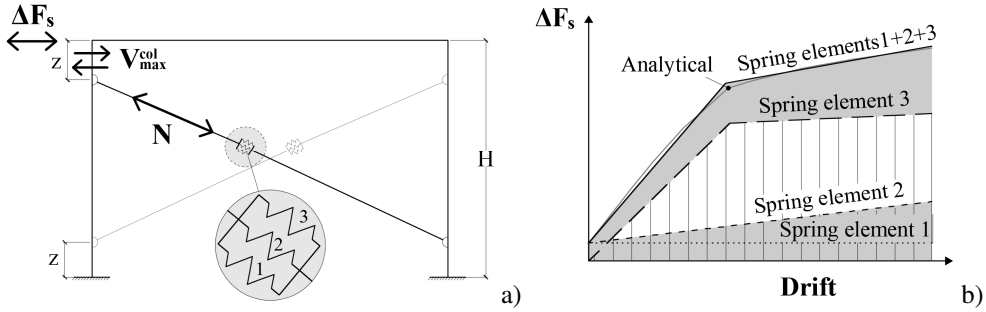

Figure 5: Simplified equivalent strut model for the infills with horizontal sliding joints: a) equivalent strut model for the infill with horizontal sliding joints; b) force-drift relationships of springs.

	Spring 1	Spring 2	Spring 3
Initial stiffness (kN/m)	8239827	345507	3900
Yielding Force (kN)	37.04	1E-05	53.47
Post-yielding stiffness (kN/m)	0	345.51	687.22

Table 4: Calibration parameters for the parallel spring elements modeling the infill with horizontal sliding joints.

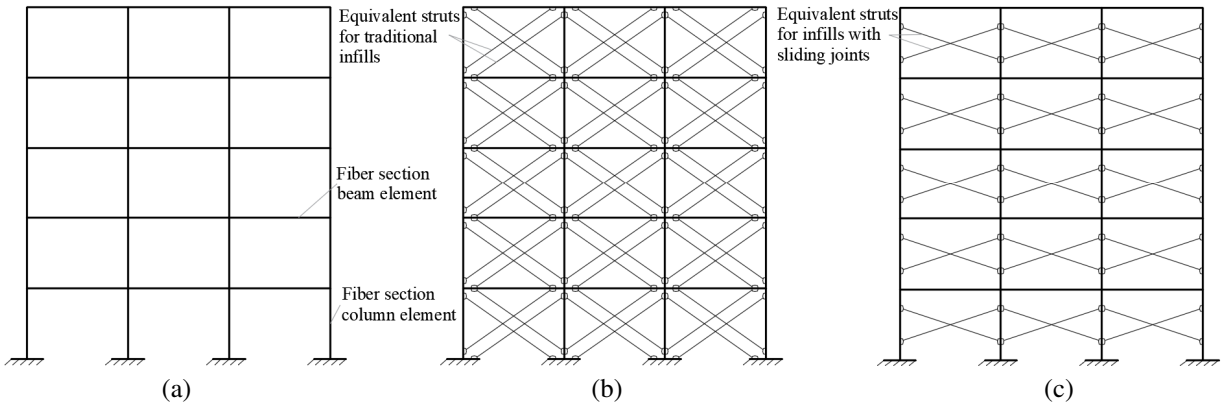

Figure 6: Layout of the case study RC frame model: a) bare frame; b) traditionally infilled frame; c) sliding-joint infilled frame.

4.2. Definition of structural and non-structural limit states

In the assessment framework the four standard PBEE limit states (namely operational limit state (O-LS), damage limitation limit state (DL-LS), life-safety limit state (LS-LS) and collapse limit state (CO-LS)) are considered. Two additional limit states are added to better characterize the different damage states. One concerns the frame initial damage (FID-LS) due to first yielding or first shear cracking, the other considers the attainment of infills severe damage (ISD-LS). Among the considered limit states, O-LS, DL-LS and ISD-LS are referred to damage of non-structural components (the infills), while FID-LS, LS-LS and CO-LS identify damage of structural elements. The standard limit states (O-LS, DL-LS, LS-LS and CO-LS) are used for EAL assessment since the associated percentage losses are calibrated [33].

The criteria adopted to define the different limit states are summarized in Table 5. As regards non-structural limit states, O-LS, DL-LS and ISD-LS are defined as function of the interstorey drift, based on the results previous experimental studies on traditional [42] and sliding-joints infills [14, 16]. For what concerns structural limit states, collapse limit state (CO-LS) is achieved in correspondence of the first of the following conditions: *i)* achievement of ultimate chord-rotation (θ_u) of columns (evaluated according to Eurocode 8 [43]), *ii)* achievement of ultimate shear capacity ($V_{R,u}$) of columns, iii) achievement of 6.5% interstorey drift, when second order effects could jeopardize the stability of the structure. In the performed analyses, an axial force-chord rotation (N-θ) interaction domain is considered, in order to take into account the variation of chord rotation capacity as a function of the variation of axial load on columns, as proposed in [31]. The ultimate shear capacity $V_{R,u}$ of column is evaluated according to the Model Code 2010 [44] expression, with unit safety coefficients for the materials to maintain the consistency with the material models used in the analysis.

The LS-LS is simply defined by the 80% of the respective θ_u and $V_{R,u}$ capacities at CO-LS. Finally, the FID-LS is related to the first occurring condition between column rebars yielding and initial shear cracking. The former condition is associated with the achievement of the yielding rotation (θ_y) of frame column, according to Eurocode 8 [39], while the first shear cracking is associated with the achievement of the resistance $V_{R,i}$, evaluated using the expressione proposed by Collins (1998) [45].

		Limit state thresholds			Considered for EAL
	Limit state	Traditional infilf	Sliding-joints infill	Bare Frame	
Non-Structural Limit states	O-LS	IDR=0.20%	IDR=2.00%	-	Yes
	DL-LS	IDR=0.50%	IDR=3.00%	-	Yes
	ISD-LS	IDR=1.50%	IDR=4.00%	-	No
Structural Limit states	FID-LS	θ_y or $V_{1st\ crack}$			No
	LS-LS	$0.8\theta_u$ or $0.8V_{Rd}$			Yes
	CO-LS	θ_u or V_{Rd} or IDR=6.5%			Yes

Table 5: Structural and non-structural limit state thresholds for traditional and sliding joint infills.

5 INCREMENTAL DYNAMIC ANALYSIS

As shown in Figure 7, a set of 30 natural ground motions is selected through the software REXEL [46] in order to get spectrum-compatibility with the design spectrum of the site of Cosenza (Italy) with soil type C and 457 years return period.

To perform IDAs, accelerograms are scaled in such a way that the respective spectra assume the same value of $S_a(T_1)$ in correspondence to the first vibration period for each considered structure. The vibration periods of the three considered structures are evaluated on the bilinear equivalent capacity curves obtained by means of preliminary pushover analyses. Vi-

bration periods of each structure are derived from the stiffness of the elastic branch of bilinear curves, by averaging results obtained for modal and uniform distributions (Table 6).

	T_1 (s)		
	Uniform distribution	Modal Distribution	Mean
Bare Frame	1.70	1.52	1.61
Frame with traditional infills	0.45	0.40	0.42
Fram with sliding-joint infills	1.43	1.29	1.36

Table 6: Determination of reference vibration period of the structures

IDA curves highlighting structural limit states are reported in Fig. 7. The overall trend shows that bare frame and sliding joint-infilled frame achieve collapse in correspondence of very similar spectral acceleration levels. Also maximum interstorey drifts recorded present similar magnitudes, ranging between 4.5% and 6.5%, which also demonstrate the trend of sliding-joint infilled frames to behave in a ductile manner with very few cases of shear collapse in the columns. A very different trend is observed for traditionally infilled frames, which present collapses at significantly higher spectral acceleration levels and noticeably reduced ultimate displacement values.

As regards frame initial damage limit state, the presence of the infill anticipates the damage activation in both the TI and the SJ case (occurred at about 0.5% and 1.5%, respectively), with respect to the BF one, for which the FID-LS is reached at about 3% drift. The difference between the performance of the two infilled configuration is related to the different stiffening effect acted by the two infill typologies.

Fig. 8 shows IDA curves highlighting non-structural limit states. For SJ and TI frames, it can be observed that *O-LS* and *DL-LS* occur at similar *IM* intensities, but for the SJ case they occur at significantly larger drift levels. As for the ISD-LS, it is achieved at about $S_a(T_1)$=1.5g for the TI frame, while it is attained for a halved *IM* in case of SJ infilled frames. Also this LS, for the SJ case, is associated with larger IDR (4%), highlighting that severe damage of SJ infills occurs in correspondence of drift levels close to those inducing collapse.

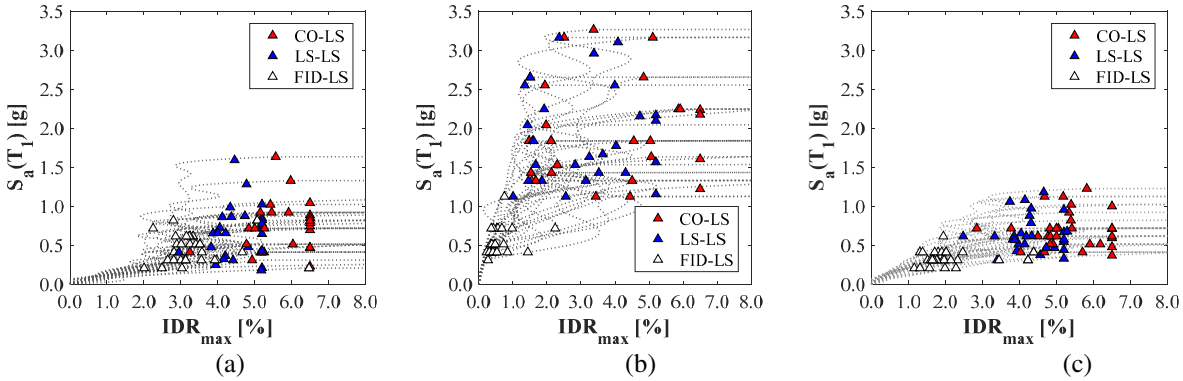

Figure 7: IDA curves and structural limit state points for: a) bare frame, b) traditionally infilled frame; c) sliding-joint infilled frame.

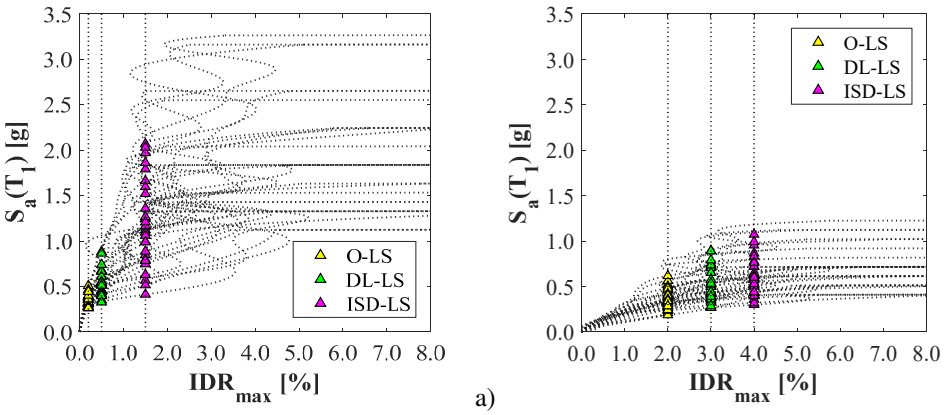

Figure 8: IDA curves and non-structural limit state points for: a) traditionally infilled frame; b) sliding-joint infilled frame.

6 HAZARD, FRAGILITY AND RELIABILITY ASSESSMENT

For the site under investigation (Cosenza, Italy) and the specified soil stiffness (type C according to EC8 classification), hazard curves, representing the annual rates of exceeding the $IM=S_a(T_1)$, are obtained for each vibration period associated with the three structural typologies. In detail, hazard curves are defined as interpolation functions of single $S_a(T_1)$-λ points, representing the values assumed by spectral accelerations at a given period for different return period design spectra ($\lambda=1/T_R$). Hazard curves are then converted into probabilities of exceeding within a service life of 50 years by using the Poisson's model equation provided in Eq. (3). The resulting hazard curves are superimposed with fragility curves of the three structural typologies (Figs. 9 and 10). The intersection areas between hazard and fragility curves are proportional to the probabilities of exceeding the different limit states, which are numerically determined by Eq. (2). Figs. 9 and 10 highlight the different amplitudes of the intersection areas between hazard and fragility curves, showing that, in the case of traditionally infilled frames, major intersection amplitudes can be recognized for both structural and non-structural limit states.

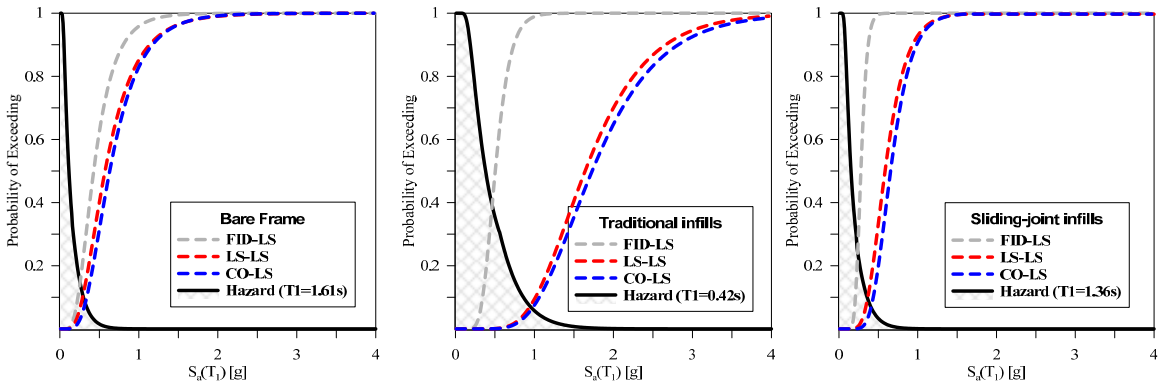

Figure 9: Fragility curves of structural limit states and hazard curves (Cosenza, Soil Type C) for: a) bare frame; b) traditionally infilled frame; c) sliding-joint infilled frame.

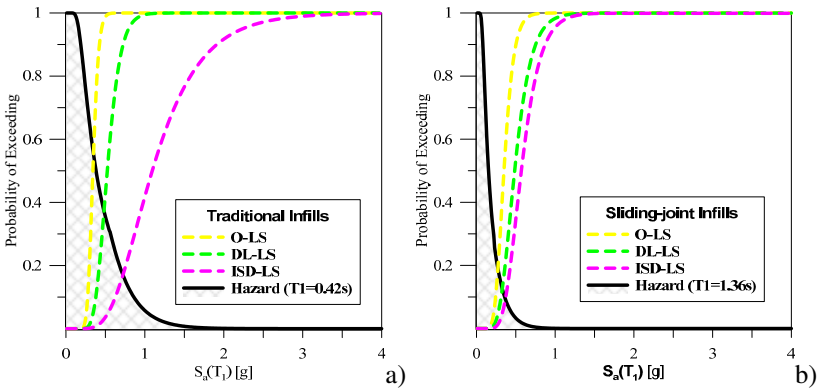

Figure 10: Fragility curves of non-structural limit states and hazard curves (Cosenza, Soil Type C) for: a) traditionally infilled frame; b) sliding-joint infilled frame.

The obtained probabilities of occurrence (P_f) for both structural and non-structural limit states are reported in Table 7. From the structural point of view, noticeable differences can be observed for the *FID-LS*, where TI frames achieve a P_f of 15%, which results 5 times and 10 times the same probabilities evaluated for SJ infilled frame and bare frame respectively. As regards LS-LS and CO-LS, the obtained probabilities of occurrence are in the same order magnitude for the three cases, with the traditionally infilled frame presenting slightly larger values. However, the largest differences are highlighted from non-structural limit states, which show a significantly reduced probability of occurrence in the cases of SJ infills with respect to TI for all the considered *LS*. Probabilities of occurrence of *O-LS*, *DL-LS* and *ISD-LS* for traditionally infilled frames are about 10 times, 13 times and 5 times the probabilities evaluated in the case sliding-joint infilled frames. This result can be justified by the reduced stiffness and shear interaction of SJ infills with the frame, which allows the attainment of non-structural *LS* at significantly larger drifts with respect to the case of TI frames. Moreover, the hazard for the SJ infilled frame is significantly lower than that of TI case, due to a longer vibration period, which is close to that of the bare frame.

		Probabilities of failure P_f (-)		
		Bare Frame	Traditional Infills	Sliding-joint infills
Non-structural LS	O-LS	-	1.72×10^{-1}	1.60×10^{-2}
	DL-LS	-	9.53×10^{-2}	7.41×10^{-3}
	ISD-LS	-	2.23×10^{-2}	4.41×10^{-3}
Structural LS	FID-LS	1.48×10^{-2}	1.50×10^{-1}	2.50×10^{-2}
	LS-LS	3.92×10^{-3}	4.77×10^{-3}	4.45×10^{-3}
	CO-LS	2.49×10^{-3}	3.95×10^{-3}	2.61×10^{-3}

Table 7: Probabilities of occurrence of limit states for the different structures.

7 LOSS ASSESSMENT

Expected annual loss assessment is carried out using the procedure by [33], updated as illustrated in section 2 and considering only the standard limit states for structural components (*LS-LS* and *CO-LS*) and non-structural components (*O-LS* and *DL-LS*). As described in section 2, the annual rates of exceeding the limit states are obtained from hazard curves ($\lambda[IM]$) using the spectral accelerations associated with the 50% probability of exceeding the limit states ($\overline{S}_{a-LS}(T_1)$) expressed by the respective fragility curves. λ_{LS} and $\overline{S}_{a-LS}(T_1)$ values are reported in Table 8, while Fig. 11 illustrates the obtained λ-*%RC* relationships for TI and SJ

cases. The obtained expected annual loss of the sliding-joint infilled frame (0.40%) is about half of the traditionally infilled frame (0.76%). This difference is entirely due to the gain in terms of reduced λ for non-structural limit states, which is one order of magnitude lower with respect to the case of traditional infills. Both TI and SJ structures have EAL lower than the reference value of 1.13%, which is associated to the ideally code conforming building. This highlights that, traditionally infilled frames design according to seismic codes have adequate performance in terms of EAL, which allow assigning an A seismic risk class according to the Italian guidelines for seismic risk classification [33]. On the other hand, the adoption of sliding-joint infills allows the achievement of the most preforming risk class (A+).

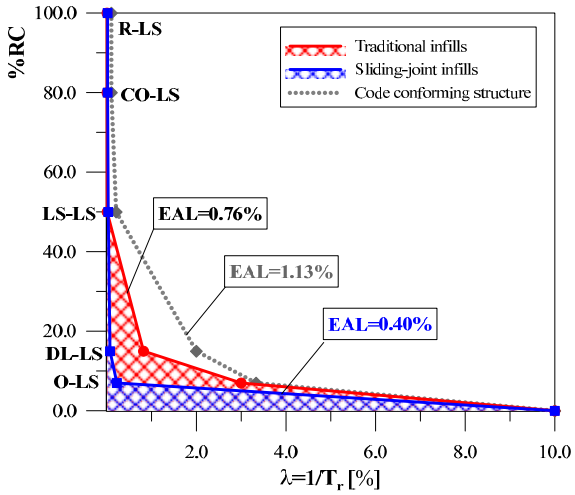

Figure 11: λ-%RC relationships and EAL for TI frames, SJI frame and code compliant reference structure.

	Traditional Infills			Sliding-joint infills		
	$\overline{S}_{a-LS}(T_1)$[g]	λ_{LS}	EAL [%]	$\overline{S}_{a-LS}(T_1)$[g]	λ_{LS}	EAL [%]
CO-LS	1.73	5.76×10^{-5}	0.76	0.66	1.84×10^{-4}	0.40
LS-LS	1.64	8.36×10^{-5}		0.59	3.24×10^{-4}	
DL-LS	0.52	8.21×10^{-3}		0.49	7.27×10^{-4}	
O-LS	0.34	1.69×10^{-2}		0.35	2.25×10^{-3}	

Table 8: $\overline{S}_{a-LS}(T_1)$ and λ_{LS} values at the different limit states and EAL values for TI frames and SJI frames.

8 CONCLUSIONS

The paper presented a PBEE approach properly defined to assess and compare the performance of infilled frames with traditional infills and innovative infills with sliding-joint subpanels. The adopted methodology is based on incremental dynamic analysis performed considering specific limit states defined to account for both structural and non-structural damage.

The performances of the systems are compared through a reliability assessment carried out by accounting for both fragility and hazard to obtain probabilities of occurrence of each considered limit state. Finally, loss analysis provided the expected annual losses during the service life for the different infilled frame typologies.

The IDA curves show that the frame infilled with the innovative sliding joint technique tends to behave similarly to the bare frame in terms of strength, stiffness and failure modes. On the contrary, the response of traditionally infilled frame is characterized by significantly increased overall resistance but, in many cases, brittle shear failures due to the large shear demand related to the stronger infill-frame interaction. As for the non-structural limit states,

their attainment is significantly delayed in SJ frames (in terms of interstorey drift) because of the reduced tendency to undergo severe damage even in case of large interstorey drifts.

Although fragility curves of TI frames apparently show a significantly better performance, similar probabilities of occurrence (*Pf*) have been obtained for life safety and collapse limit-states for the three considered cases. On the contrary, large reliability differences are observed for non-structural limit states, where P_f of *O-LS*, *DL-LS* and *ISD-LS* for traditionally infilled frames was about 10 times, 13 times and 5 times the same probabilities evaluated in for SJI frames. Such reliability differences are due to the lower damage suffered by SJ infills with respect to TI frames, even for of large drifts, and also to the lower hazard associated with the longer vibration period of SJ infilled frames.

The performed expected annual loss assessment allows evaluating, for SJ infilled frames, an EAL equal to 0.40%, that is about a half of that of traditionally infilled frames (0.76%). This gain is entirely related to the reduced annual rates of exceeding evaluated for non-structural limit states in case of SJ infilled frames.

As a conclusion, the reported assessment highlights that frames infilled with the sliding joints technique results an effective design solution to improve reliability and reduce losses during the service life of masonry infilled RC structures.

9 ACKNOWLEDGEMENTS

This study was supported by ReLUIS, Rete di Laboratori Universitari di Ingegneria Sismica, WP 10, 2019-2021.

10 REFERENCES

[1] F. Braga, V. Manfredi, A. Masi, A. Salvatori, M. Vona. Performance of non-structural elements in RC buildings during the L'Aquila, 2009 earthquake, *Bull Earth Eng*, **9(1)**, 307–324, 2011.

[2] G. De Martino, M. Di Ludovico, A. Prota, C. Moroni, G. Manfredi, M. Dolce. Estimation of repair costs for RC and masonry residential buildings based on damage data collected by post-earthquake visual inspection, *Bull Earth Eng*, **15(4)**,1681–1706, 2017.

[3] C. Del Vecchio, M. Di Ludovico, S. Pampanin, A. Prota. Repair costs of existing RC buildings damaged by the L'Aquila earthquake and comparison with FEMA P-58 predictions, *Earthq Spectra,* **34(1)**, 237–263, 2018.

[4] P.G. Asteris, L. Cavaleri, F. Di Trapani, A.K. Tsaris. Numerical modelling of out-of-plane response of inflled frames: state of the art and future challenges for the equivalent strut macromodels, *Engineering Structures*, **132**, 110–122, 2017.

[5] F. Di Trapani, P.B. Shing, L. Cavaleri. Macroelement Model for In-Plane and Out-of-Plane Responses of Masonry Infills in Frame Structures, *Journal of Structural Engineering*, **144(2)**, 04017198, 2018.

[6] M. Preti, V. Bolis. Seismic analysis of a multi-story RC frame with infills partitioned by sliding joints, *Ingengeria sismica*, **34(3-4)**, 175–187, 2017.

[7] L. Cavaleri, F. Di Trapani, P.G. Asteris, V. Sarhosis. Influence of column shear failure on pushover based assessment of masonry infilled reinforced concrete framed structures: a case study, *Soil Dynamics and Earthquake Engineering*, **100**, 98–112, 2017.

[8] A. Fiore, G. Spagnoletti, R. Greco. On the prediction of shear brittle collapse mechanisms due to the infill-frame interaction in RC buildings under pushover analysis, *Engineering Structures*, **121**, 147-159, 2016.

[9] R. Greco, A. Fiore, G.C. Marano. The role of modulation function in nonstationary stochastic earthquake model, *Journal of Earthquake and Tsunami*, **8(5)**, 1450015, 2014.

[10] I. Koutromanos, M. Kyriakides, A.Stavridis, S. Billington, P.B. Shing. Shake-table tests of a three-story masonry-infilled RC frame retrofitted with composite materials, *Journal of Structural Engineering,* **139(8)**, 1340-1351, 2013

[11] P. Ezzatfar, B. Binici, O. Kurc, E. Canbay, H. Sucuoglu, G.Ozcebe. Application of mesh reinforced mortar for performance enhancement of hollow clay tile infill walls, *Seismic Evaluation and Rehabilitation of Structures*, Springer, **26**, 171-186, 2014.

[12] A.V. Tsantilis, T.C. Triantafillou. Innovative seismic isolation of masonry infills using cellular materials at the interface with the surrounding RC frames, *Engineering Structures*, **155**, 279–297, 2018.

[13] M. Mohammadi, V. Akrami, R. Mohammadi-Ghazi. Methods to Improve Infilled Frame Ductility, *Journal of Structural Engineering*, **137(6)**, 646–653, 2011.

[14] M. Preti, V. Bolis, A. Stavridis. Design of masonry infill walls with sliding joints for earthquake structural damage control, *Proceedings of the 16th International Brick and Block Masonry Conference, IBMAC*, Padua, Italy, 2016.

[15] M. Preti, M. Neffati, V.Bolis. Earthen masonry infill walls: Use of wooden boards as sliding joints for seismic resistance, *Construction and Building Materials*, **184**, 100–110, 2018.

[16] X. Gao, A. Stavridis, V. Bolis, M. Preti. Experimental study on the seismic performance of non-ductile rc frames infilled with sliding subpanels, *Proccedings of Eleventh U.S. National Conference on Earthquake Engineering Integrating Science, Engineering & Policy*, Los Angeles, California, 2018.

[17] X. Palios, M.N. Fardis, E. Strepelias, S.N. Bousias. Unbonded brickwork for the protection of infills from seismic damage, *Engineering Structures*, **131**, 614–624, 2017.

[18] C.F. Manzini, P.Morandi, R.R. Milanesi, G. Magenes. Shaking-table test on a two-storey RC framed structure with innovative infills with sliding joints, *Proceedings of 16th European conference on earthquake engineering*, Thessaloniki, Greece, 2018.

[19] V. Bolis, A. Stavridis, M. Preti. Numerical Investigation of the In-Plane Performance of Masonry-Infilled RC Frames with Sliding Subpanels, *Journal of Structural Engineering*, **143(2)**, 04016168, 2017.

[20] M. Preti, V. Bolis, A. Stavridis. Seismic infill–frame interaction of masonry walls partitioned with horizontal sliding joints: analysis and simplified modeling, *Journal of Earthquake Engineering*, 1–27, 2017.

[21] D. Vamvatsikos, A.C. Cornell. Incremental dynamic analysis, *Earthq Eng Struct Dyn* **31(3)**,491–514, 2002.

[22] C.A.Cornell, H. Krawinkler. Progress and challenges in seismic performance assessment. PEER Center News 3, University of California, Berkeley, 2000.

[23] P. Castaldo, G. Mancini, B. Palazzo. Seismic reliability-based robustness assessment of three-dimensional reinforced concrete systems equipped with single-concave sliding devices, *Engineering Structures* **163**, 373-387, 2018.

[24] P. Castaldo, M. Ripani, R.L. Priore, Influence of soil conditions on the optimal sliding friction coefficient for isolated bridges, *Soil Dynamics and Earthquake Engineering,* **111**, 131-148, 2018.

[25] P. Castaldo, F. Jalayer, B. Palazzo. Probabilistic assessment of groundwater leakage in diaphragm wall joints for deep excavations, *Tunnelling and Underground Space Technology,* **71**, 531-543, 2018.

[26] P. Castaldo, M. Calvello, B. Palazzo. Probabilistic analysis of excavation-induced damages to existing structures, *Computers and Geotechnics*, **53**, 17-30 , 2013.

[27] P. Castaldo, B. Palazzo, T. Ferrentino, G. Petrone. Influence of the strength reduction factor on the seismic reliability of structures with FPS considering intermediate PGA/PGV ratios, *Composites Part B: Engineering*, **115**, 308-315, 2017,

[28] F. Basone, P. Castaldo, L. Cavaleri, F. Di Trapani. Response spectrum analysis of frame structures: reliability-based comparison between complete quadratic combination and damping-adjusted combination, *Bulletin of Earthquake Engineering*, **17(5)**, 2687-2713, 2019.

[29] L. Cavaleri, F. Di Trapani, G. Macaluso, M. Papia. Reliability of code proposed models for assessment of masonry elastic moduli, *Ingegneria Sismica*, 29(1), 38–59, 2012.

[30] F. Basone, L. Cavaleri, F. Di Trapani, G. Muscolino. Incremental dynamic based fragility assessment of reinforced concrete structures: Stationary vs. non-stationary artificial ground motions. *Soil Dynamics and Earthquake Engineering,* **103**, 105–117, 2017.

[31] F. Di Trapani, M. Malavisi. Seismic fragility assessment of infilled frames subject to mainshock/aftershock sequences using a double incremental dynamic analysis approach, *Bulletin of Earthquake Engineering*, **17(1)**, 211-235, 2019

[32] Calvi GM. Choices and criteria for seismic strengthening. *J Earthq Eng*, **17**, 769–802, 2013.

[33] E. Cosenza, C. Del Vecchio, M. Di Ludovico, M. Dolce, C. Moroni, A. Prota, E. Renzi. The Italian guidelines for seismic risk classification of constructions: technical principles and validation, *Bulletin of Earthquake Engineering,* **16(12)**, 5905-5935, 2018.

[34] Ministry Decree, January 17th, 2018. Norme tecniche per le costruzioni (Technical codes for construction) [in Italian], 2018.

[35] P.G. Asteris, L. Cavaleri, F. Di Trapani, V. Sarhosis. A macro-modelling approach for the analysis of infilled frame structures considering the effects of openings and vertical loads, *Structure and Infrastructure Engineering*, **12(5)**, 551–566, 2016.

[36] V. Bolis, M. Preti. Openigns in infills with horizontal sliding joints: a parametric study to support the design, *Bulletin of Earthquake Engineering*, Submitted for publication., 2019.

[37] F. McKenna, G.L. Fenves, M.H. Scott. Open system for earthquake engineering simulation," University of California, Berkeley, CA, 2000.

[38] G. Campione, L. Cavaleri, F. Di Trapani, G. Macaluso, G. Scaduto. Biaxial deformation and ductility domains for engineered rectangular RC cross-sections: a parametric study highlighting the positive roles of axial load, geometry and materials, *Engineering Structures*, **107(15)**, 116–134, 2016.

[39] G. Campione, L. Cavaleri, F. Di Trapani, M.F. Ferrotto. Frictional effects in structural behavior of no end-connected steel-jacketed RC columns: experimental results and new approaches to model numerical and analytical response, *Journal of Structural Engineering*, **143(8)**, 04017070, 2017.

[40] G. Minafò, F. Di Trapani, G. Amato. Strength and ductility of RC jacketed columns: A simplified analytical method, *Engineering Structures*, 122, 184-195, 2016.

[41] F. Di Trapani, G. Bertagnoli, M.F. Ferrotto, Gino, D. Empirical Equations for the Direct Definition of Stress–Strain Laws for Fiber-Section-Based Macromodeling of Infilled Frames, *Journal of Engineering Mechanics*, **144(11)**, 04018101, 2018.

[42] P. Morandi, S. Hak, G. Magenes. Performance-based interpretation of in-plane cyclic tests on RC frames with strong masonry infills, *Engineering Structures*, **156**, 503–521, 2018.

[43] Eurocode 8 (2004) Design of structures for earthquake resistance—Part 1: general rules, seismic actions and rules for buildings. European Committee for Standardization, Brussels, 2004.

[44] Fédération internationale du béton (FIB). Model code 2010: final draft, International Federation for Structural Concrete, 2012.

[45] Collins M.P. Procedures for Calculating the Shear Response of Reinforced Concrete Elements: A Discussion, *Journal of Structural Engineering*, 124(12), 1485–1488, 1998.

[46] I. Iervolino, C. Galasso, E. Cosenza. REXEL: computer aided record selection for code-based seismic structural analysis, *Bull of Earthquake Eng*, **8**, 339-362, 2009.